Supporting Information

Activated carbon clothes for wide-voltage high-energy-density aqueous symmetric supercapacitors

Kwadwo Asare Owusu[a], Zhaoyang Wang[a], Longbing Qu[b], Zi'ang Liu[a], Jaafar Abdul-Aziz Mehrez[a], Qiulong Wei[c], Liang Zhou [a,*], Liqiang Mai [a,*]

[a]*State Key Laboratory of Advanced Technology for Materials Synthesis and Processing, Wuhan University of Technology, Wuhan 430070, China*
[b]*Department of Mechanical Engineering, The University of Melbourne, Parkville, VIC 3010, Australia.*
[c]*Department of Materials Science and Engineering, University of California Los Angeles, CA 90095 – 1595, USA.*

Experimental

Activation of carbon clothes

Activation of CCs. The CC was purchased from Shanghai Hesen Electric Co., Ltd. Before the activation process, the CC (4 × 5 × 0.031 cm^3) was ultrasonicated in acetone, ethanol, and water respectively for 20 minutes to get rid of surface impurities. The activation process was carried out by calcining the CC at 400 ^oC for 6 hours with a ramp rate of 2 $^oC\ min^{-1}$ in air. The mass density of the activated CC is calculated to be 13 mg cm^{-2}. As control experiments, pristine CCs were calcined at different temperatures and time lengths (300 ^oC for 6 hours, 400 ^oC for 2 hours, and 500 ^oC for 6 hours) to study the influence of calcination conditions on the electrochemical performance.

Material characterization

Raman spectra were obtained using a Renishaw INVIA micro-Raman spectroscopy system with a laser power of 100 mW and a spot size of 1 μm. SEM images were collected with a JEOL-7100F microscope. TEM images were recorded using a JEM-2100F STEM/EDS microscope. The Brunauer–Emmett–Teller (BET) surface area was measured using a Tristar II 3020 instrument at 77 K. XPS measurements were performed using a VG Multi Lab 2000 instrument. The adsorption curves were analyzed using NLDFT models to obtain the pore-size

* Corresponding author.
E-mail address: liangzhou@whut.edu.cn
* Corresponding author.
E-mail address: mlq518@whut.edu.cn

distribution curves. The contact angle measurements were performed using an OCA Automatic contact angle measurement device.

Electrochemical characterization

All the electrochemical measurements were performed with an electrochemical workstation (CHI 760E). Electrochemical properties of the single electrodes were first measured in a three-electrode cell system in 1 M Na_2SO_4 aqueous electrolyte. As-prepared CC (1 cm^2), platinum plate, and saturated calomel electrode were used as the working, counter and reference electrode, respectively. A symmetric electrochemical capacitor was fabricated using a coin cell with two activated carbon cloth electrodes separated by an NKK separator in 1 M Na_2SO_4 electrolyte and tested under a two-electrode system. Before fabrication, the activated carbon clothes were immersed in the aqueous electrolyte for an hour and 3 to 4 drops of electrolyte were dropped on the NKK separator. Electrochemical impedance spectroscopy was performed under a sinusoidal signal at open circuit potential over a frequency range from 0.01 to 10^5 Hz with a magnitude of 10 mV. The constant float voltage method was carried out to test the stability of the fabricated carbon symmetric device using a battery test system (LAND CT2001A).

Calculation methods

Calculation of Specific Areal and Volumetric Capacitances in a Three-Electrode System:

The areal capacitances of the working electrodes were calculated from the cyclic voltammetry curves using the equation shown below:

$$C_A = \frac{\int I \, dV}{v\Delta V} \tag{1}$$

where C_A (mF cm^{-2}) is the areal capacitance, I (A) is the discharge current, v is the scan rate and ΔV is the operating discharge potential range.

The areal capacitances of the working electrodes were calculated from the galvanostatic charge/discharge curves using the equation shown below.

$$C_A = \frac{I\Delta t}{S\Delta V} \tag{2}$$

$$C_V = \frac{I\Delta t}{V\Delta V} \quad (3)$$

where C_A (mF cm^{-2}) is the specific capacitance, I (A) is the discharge current, Δt (s) is the discharge time, S is the surface area (1 cm^2) of the carbon cloth electrode, ΔV is the operating voltage (obtained from the discharge curves excluding the potential drop) and V is the volume (0.031 cm^3) of the carbon cloth electrode.

Calculation of Specific gravimetric, areal and volumetric capacitance in a two-electrode system: The gravimetric, areal and volumetric capacitances of the single electrode in a two-electrode system were calculated using the equations shown below.

$$C_S(F\ g^{-1}) = \frac{2I\Delta t}{m\Delta V} \quad (4)$$

$$C_A(F\ cm^{-2}) = \frac{2I\Delta t}{S\Delta V} \quad (5)$$

$$C_V(F\ cm^{-3}) = \frac{2I\Delta t}{V\Delta V} \quad (6)$$

where C_S (F g^{-1}) is the gravimetric capacitance, C_A (F cm^{-2}) is the areal capacitance, C_V (F cm^{-3}) is the volumetric capacitance, I (A) is the discharge current, Δt (s) is the discharge time, m is the mass of the carbon clothes, S is the surface area (1 cm^2) of the carbon cloth electrode, ΔV is the operating voltage (obtained from the discharge curves excluding the potential drop) and V is the volume of the carbon cloth electrode.

Calculation of Specific gravimetric, areal and volumetric capacitance of the supercapacitor device: The specific capacitance of the assembled symmetric supercapacitor cell was evaluated using the equations shown below:

$$C_{ST}(F\ g^{-1}) = \frac{C_S}{4} \quad (7)$$

$$C_{AT}(F\ cm^{-2}) = \frac{C_A}{4} \quad (8)$$

$$C_{VT}(F\ cm^{-3}) = \frac{C_V}{4} \quad (9)$$

where C_S and C_{ST} ($F\ g^{-1}$) are the gravimetric capacitance of the electrode and assembled symmetric supercapacitor, respectively, C_A and C_{AT} ($F\ cm^{-2}$) are the areal capacitance of the electrode and assembled symmetric supercapacitor, respectively and C_V and C_{VT} ($F\ cm^{-3}$) are the volumetric capacitance of the electrode and assembled symmetric supercapacitor, respectively.

Calculation of energy and power density of the supercapacitor device: The energy and power density of the assembled symmetric supercapacitor were calculated using the equations shown below:

$$E_T(Wh\ kg^{-1}; \text{Wh}\ cm^{-3}; Wh\ cm^{-2}) = 0.5C_T V^2 \quad (10)$$

$$P_T(W\ kg^{-1}; \text{W}\ cm^{-3}; W\ cm^{-2}) = \frac{3600E_T}{\Delta t} \quad (11)$$

where E_T ($Wh\ cm^{-3}$; $Wh\ cm^{-2}$; $Wh\ kg^{-1}$) is the energy density, P_T ($W\ cm^{-3}$; $W\ cm^{-2}$; $W\ kg^{-1}$) is the power density, C_T ($F\ cm^{-3}$; $F\ cm^{-2}$; $F\ g^{-1}$) is the capacitance of the symmetric supercapacitor device, V is the operating potential window of the supercapacitor and Δt (s) is the discharge time.

Calculation of resistance from the voltage drop: The resistance was calculated from the galvanostatic discharge curves by dividing the voltage drop using the formula shown below:

$$R = \frac{V_{drop}}{2I} \tag{12}$$

Float Voltage Test: The constant float voltage method was carried out to test the stability of the fabricated carbon symmetric device using a battery test system (LAND CT2001A). In brief, a constant voltage of 2 V was applied to an assembled supercapacitor device with the CC-400 ^{o}C-6h electrodes and 1 M Na_2SO_4 electrolyte. Charge/discharge cycles from 0.1 to 2.0 V were performed at a constant current density of 2 mA cm^{-2} every 10 hours to quantify the corresponding retaining areal capacitance. The total test time was 300 hours.

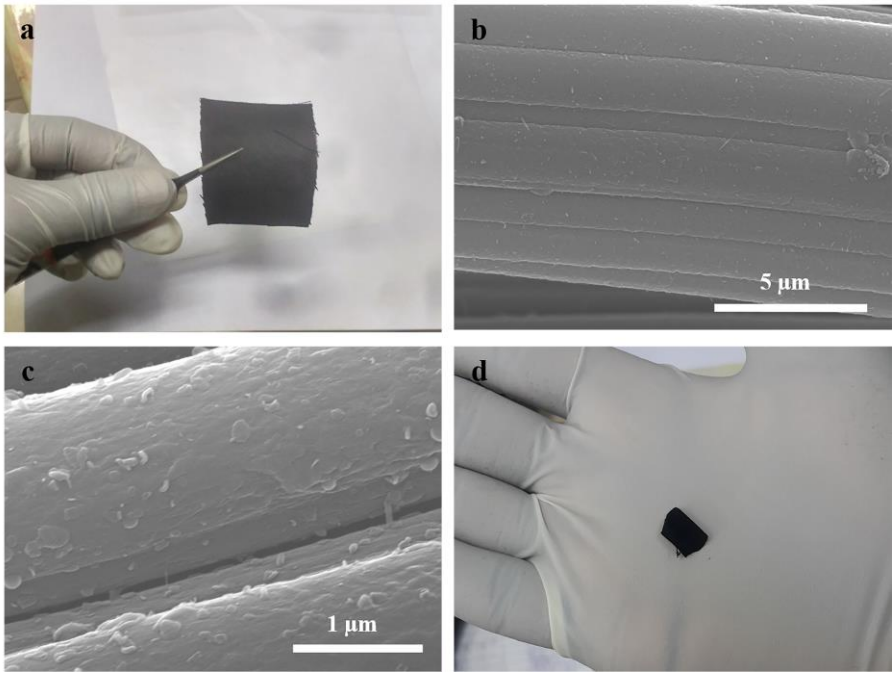

Fig. S1. (a) Optical photo of CC-400 ºC-6h. (b) SEM image of CC-300 ºC-6h. (c) SEM image of CC-400 ºC-2h. (d) Optical photo of shriveled CC-500 ºC-6h.

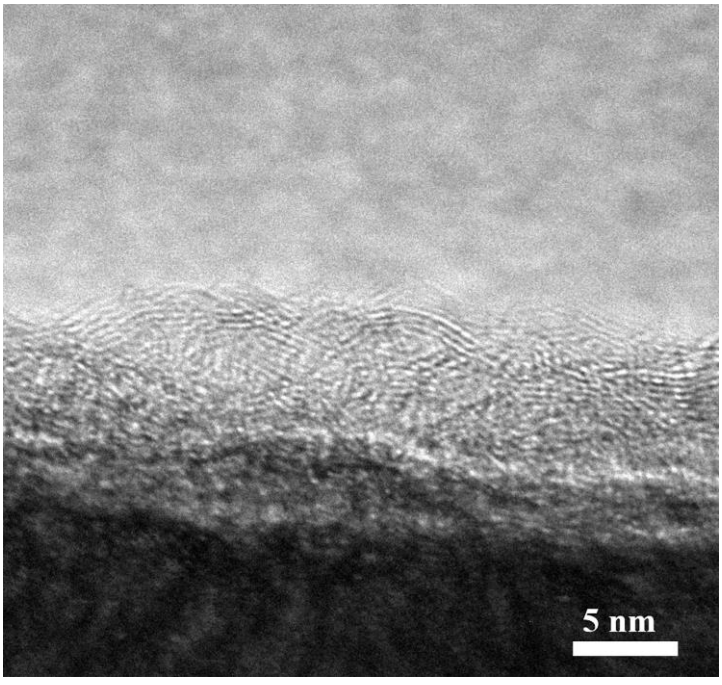

Fig. S2. HRTEM image of the activated CC.

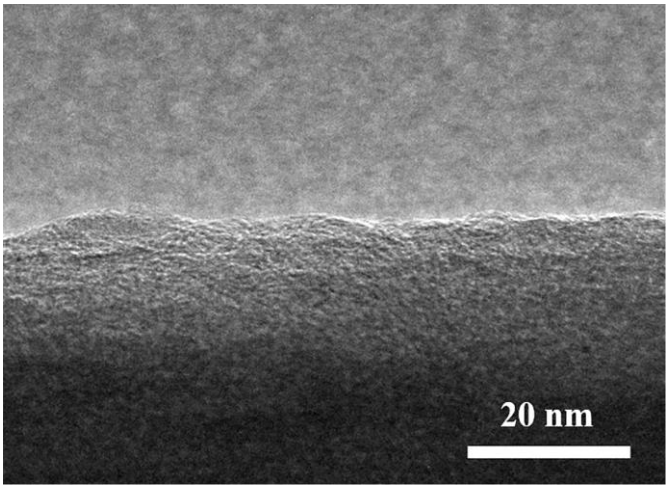

Fig. S3. TEM image of the pristine CC

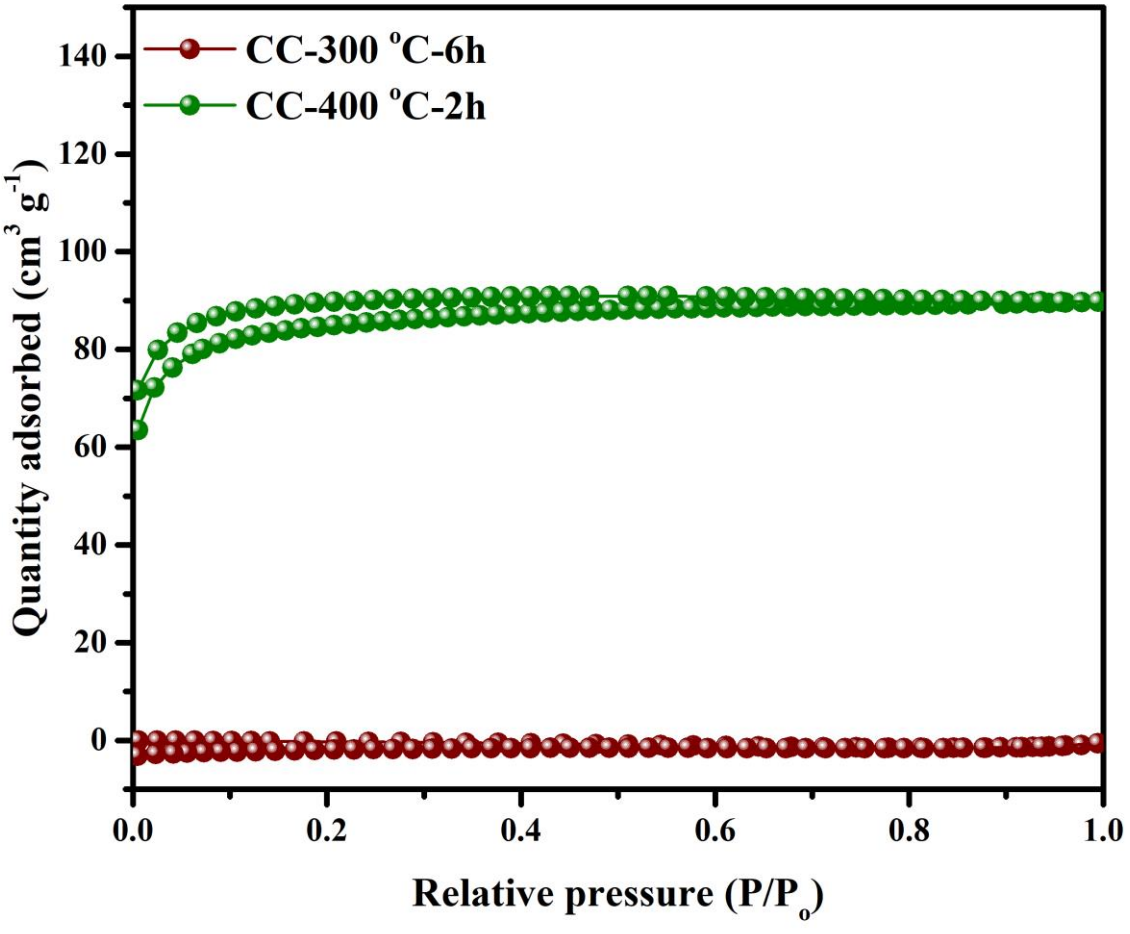

Fig. S4. N_2 adsorption-desorption isotherms of CC-300 ºC-6h and CC-400 ºC-2h.

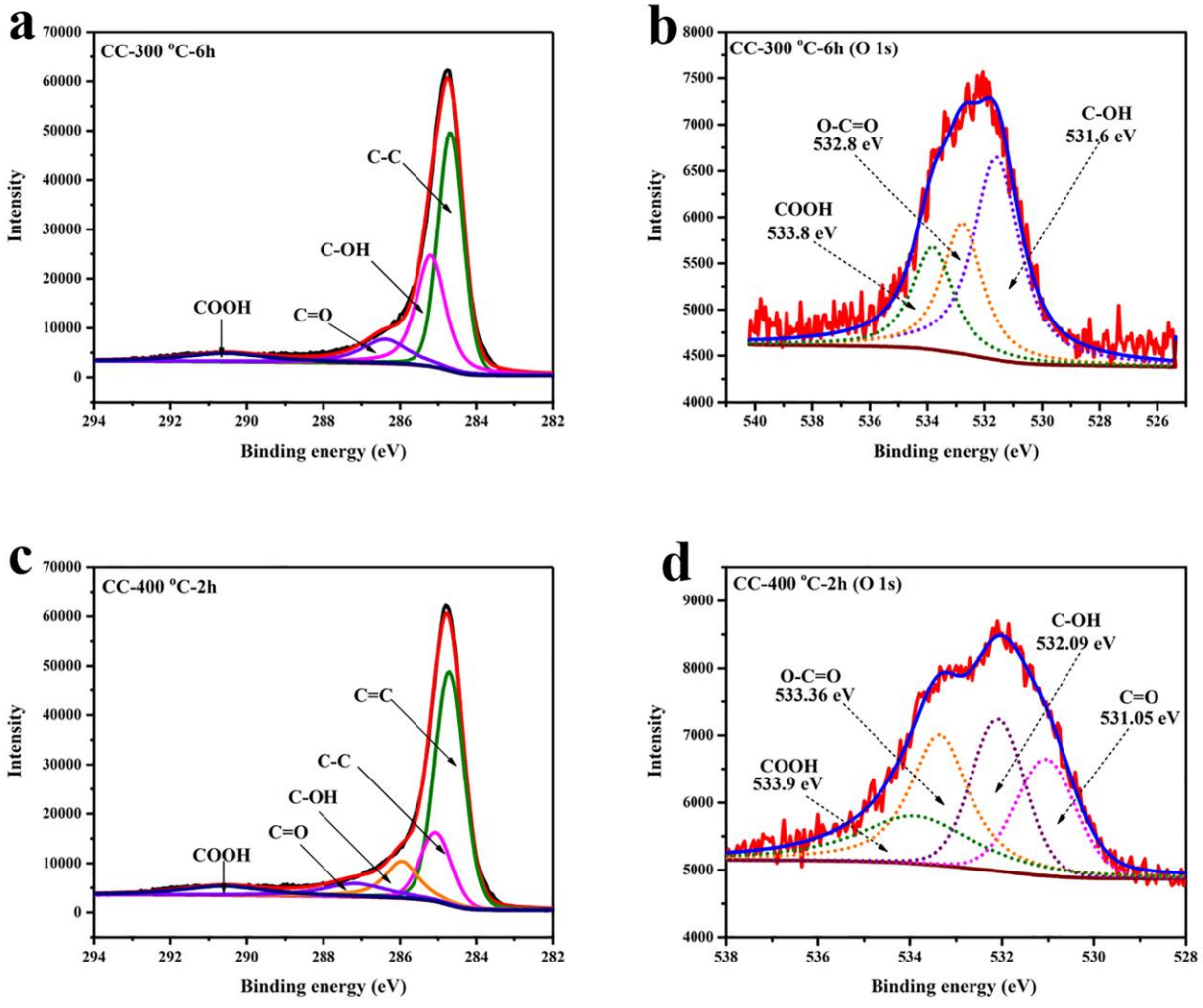

Fig. S5. (a) Deconvolution of the C 1s spectrum of the CC-300 °C-6h. (b) Deconvolution of the O 1s spectrum of the CC-300 °C-6h. (c) Deconvolution of the C 1s spectrum of the CC-400 °C-2h. (d) Deconvolution of the O 1s spectrum of the CC-400 °C-2h.

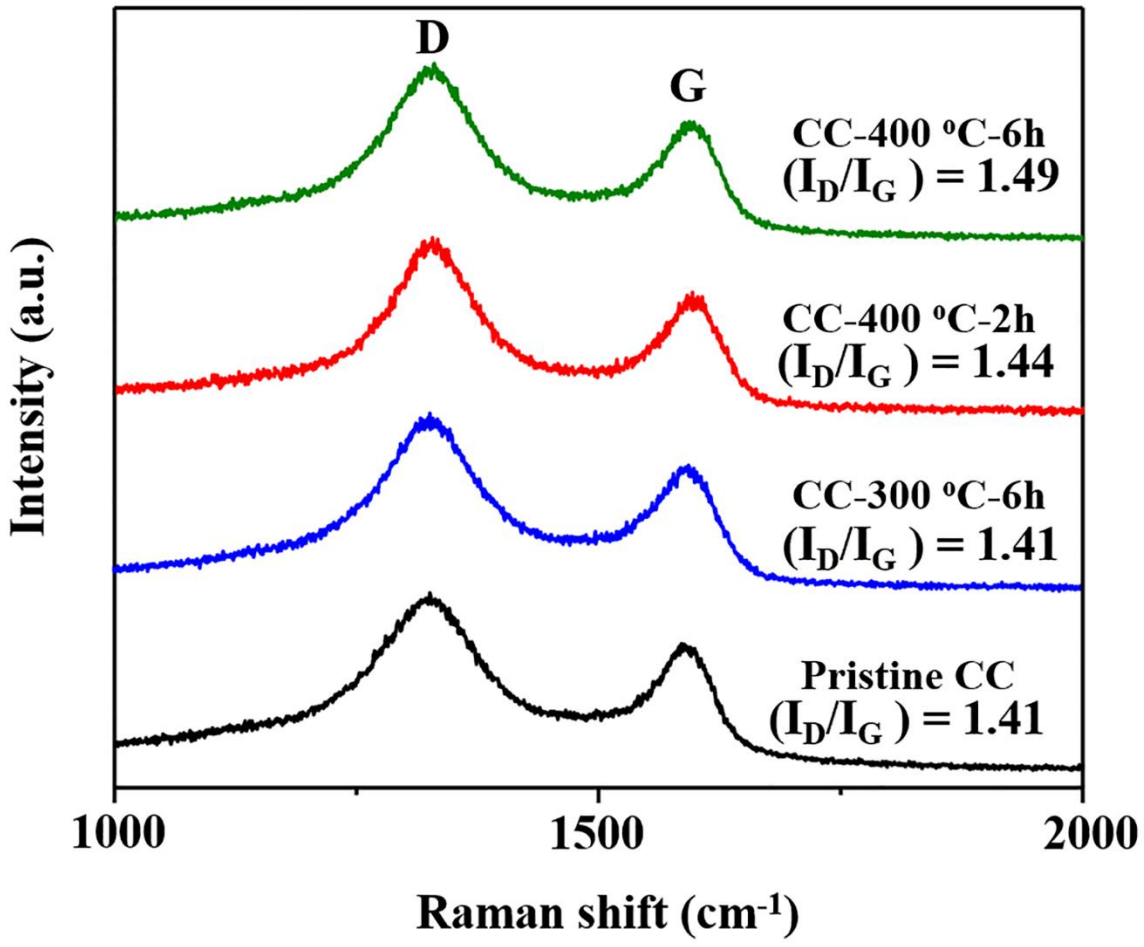

Fig. S6. Raman Spectra of the different carbon clothes showing the D and G bands.

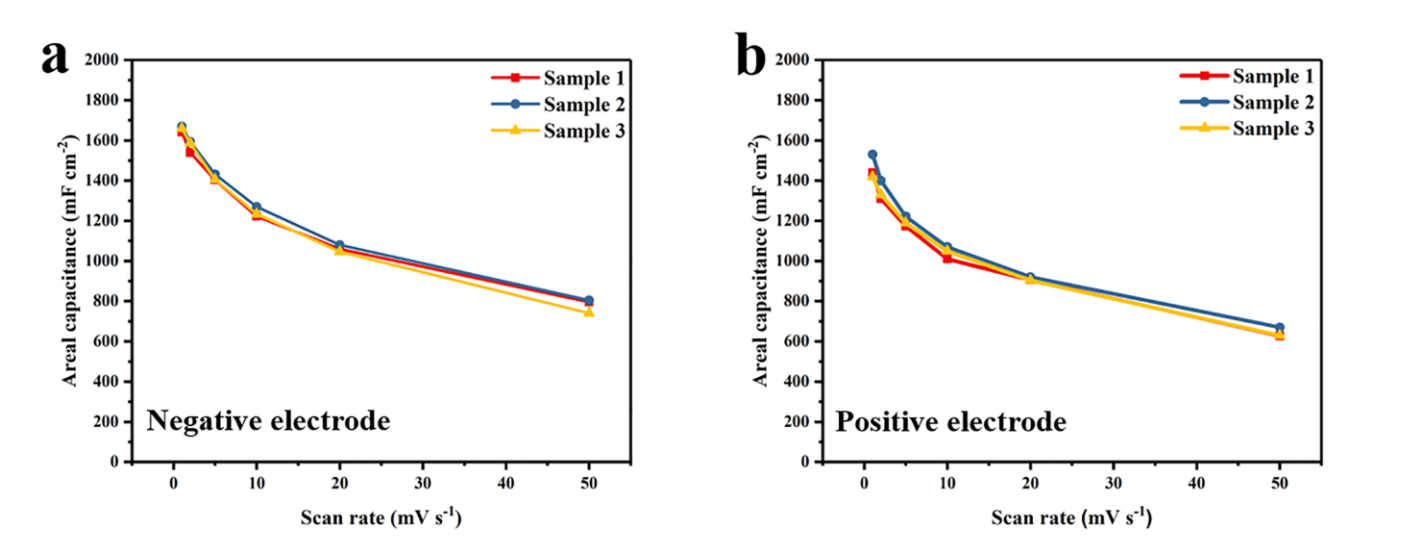

Fig. S7. (a) Areal capacitance of the CC-400 ºC-6h negative electrode at different scan rates. (b) Areal capacitance of the CC-400 ºC-6h positive electrode at different scan rates.

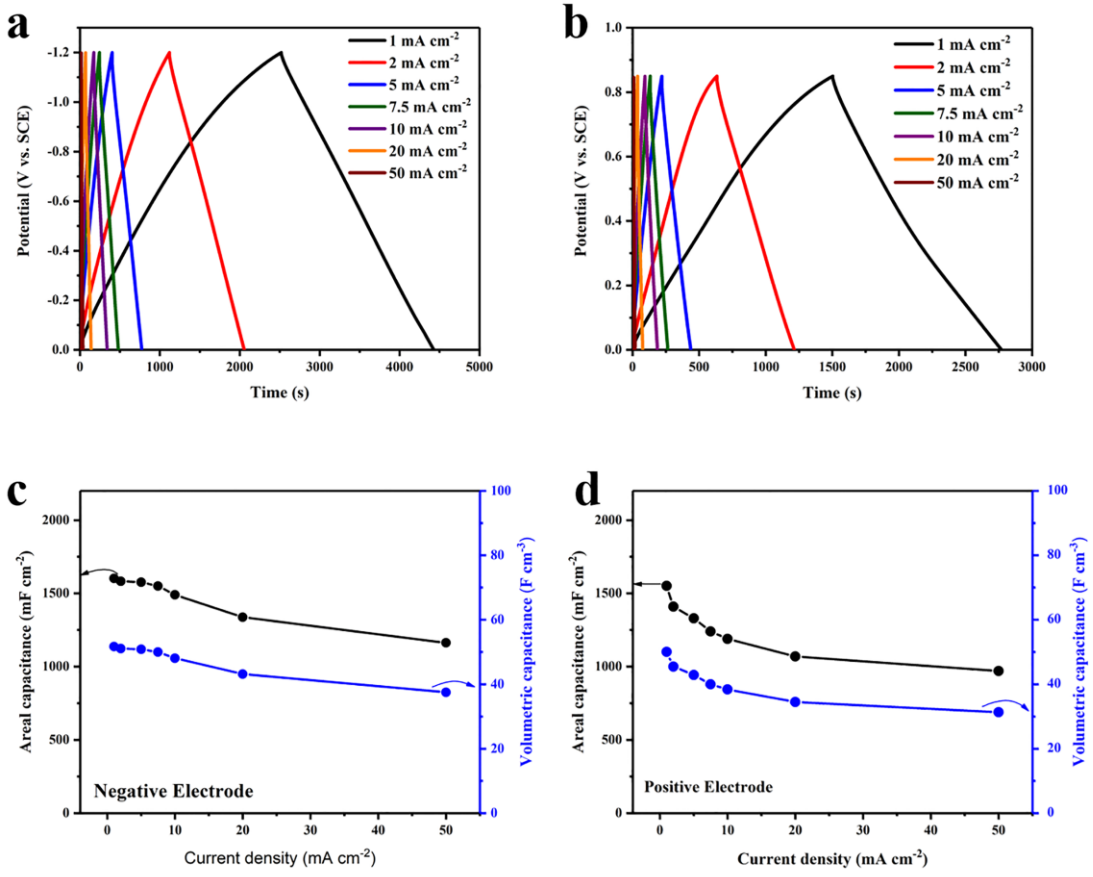

Fig. S8. (a) Charge/discharge curves of CC-400 ºC-6h at different current densities in a -1.2 – 0 V potential window. (b) Charge/discharge curves of CC-400 ºC-6h at different current densities in a 0 – 0.85 V potential window. (c) Areal and volumetric capacitances of the activated CC negative electrode at different current densities. (d) Areal and volumetric capacitances of the activated CC positive electrode as a function of current density.

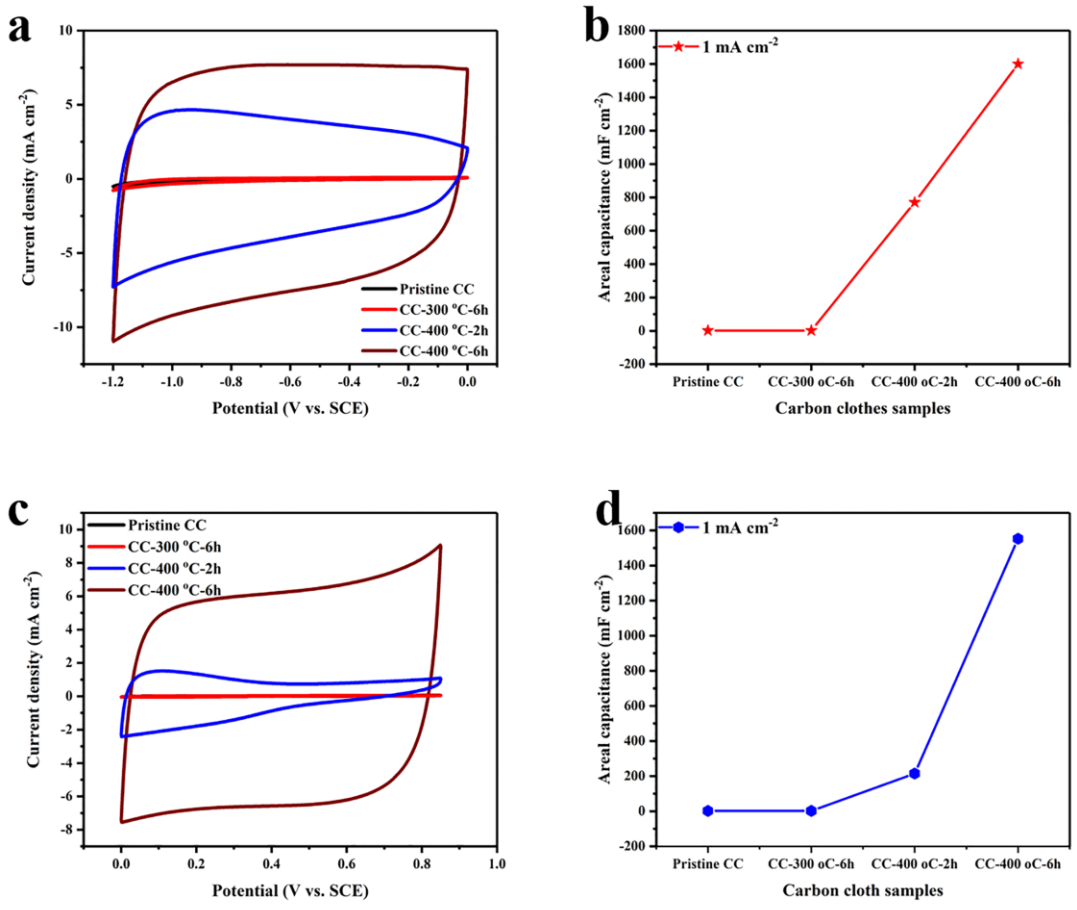

Fig. S9. (a) Cyclic voltammetry curves of pristine CC, CC-300 °C-6h, CC-400 °C-2h, and CC-400 °C-6h negative electrodes at 5 mV s^{-1}. (b) Areal capacitances of pristine CC, CC-300 °C-6h, CC-400 °C-2h, and CC-400 °C-6h negative electrodes at 1 mA cm^{-2}. (c) Cyclic voltammetry curves of pristine CC, CC-300 °C-6h, CC-400 °C-2h, and CC-400 °C-6h positive electrodes at 5 mV s^{-1}. (d) Areal capacitances of pristine CC, CC-300 °C-6h, CC-400 °C-2h, and CC-400 °C-6h positive electrodes at 1 mA cm^{-2}.

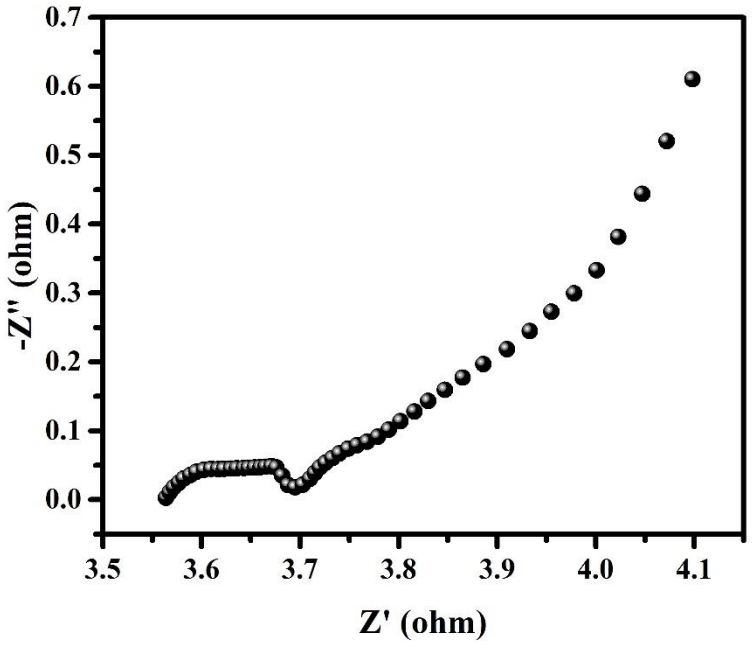

Fig. S10. Nyquist plot of the activated CC at high frequencies.

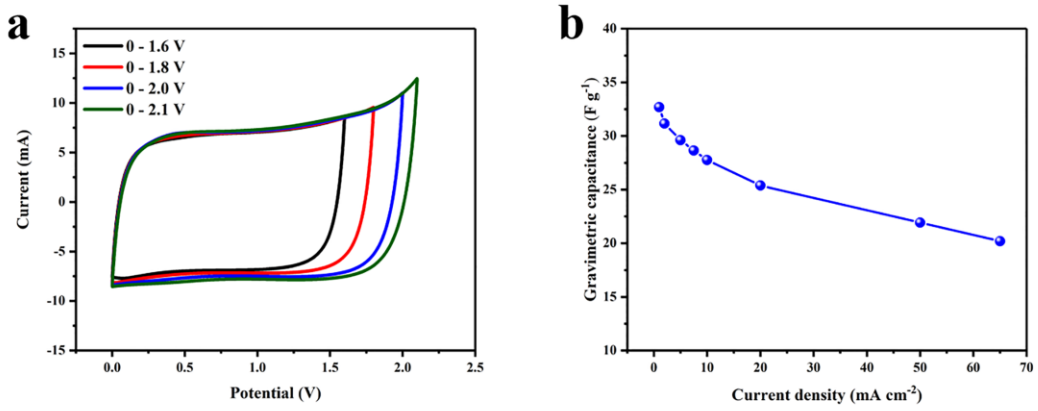

Fig. S11. Specific gravimetric capacitance of the CC-400 ºC-6h-based symmetric supercapacitor at different current densities.

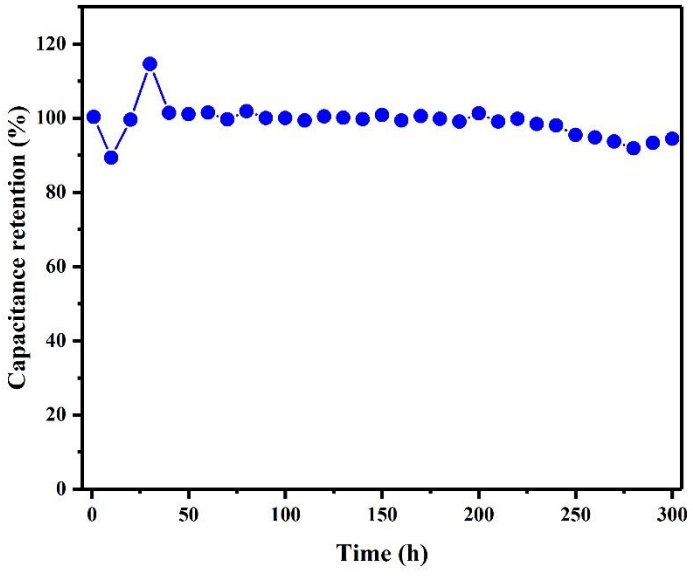

Fig. S12. Float voltage test in 1 M Na_2SO_4 electrolyte.

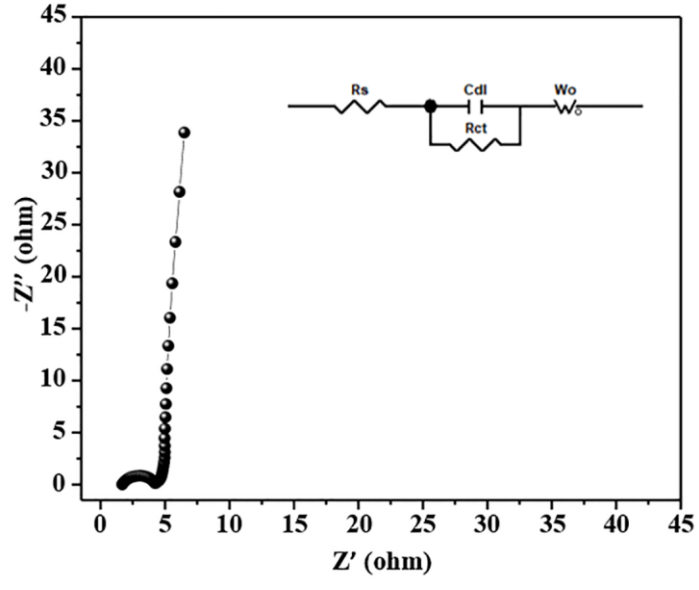

Fig. S13. Nyquist plot of the activated CC based symmetric electrochemical capacitor.

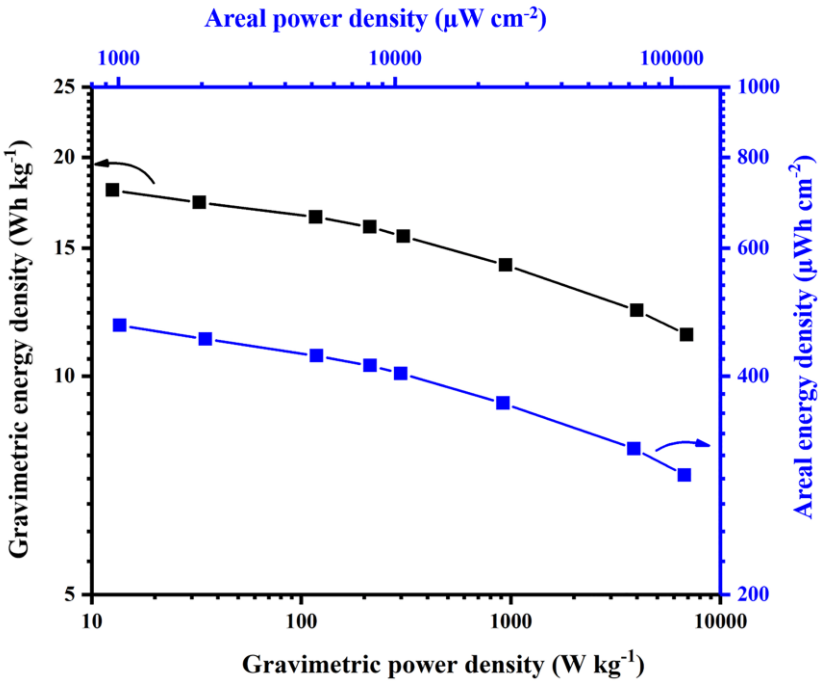

Fig. S14. The areal and gravimetric energy densities of the activated CC-based aqueous symmetric supercapacitor at different areal and gravimetric power densities.

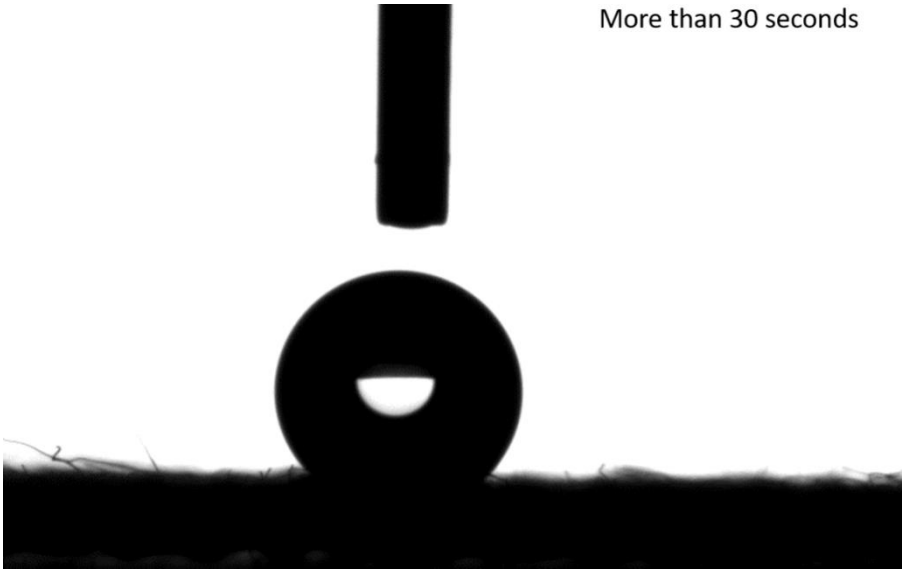

Fig. S15. Dynamic water contact angle measurement for pristine CC.

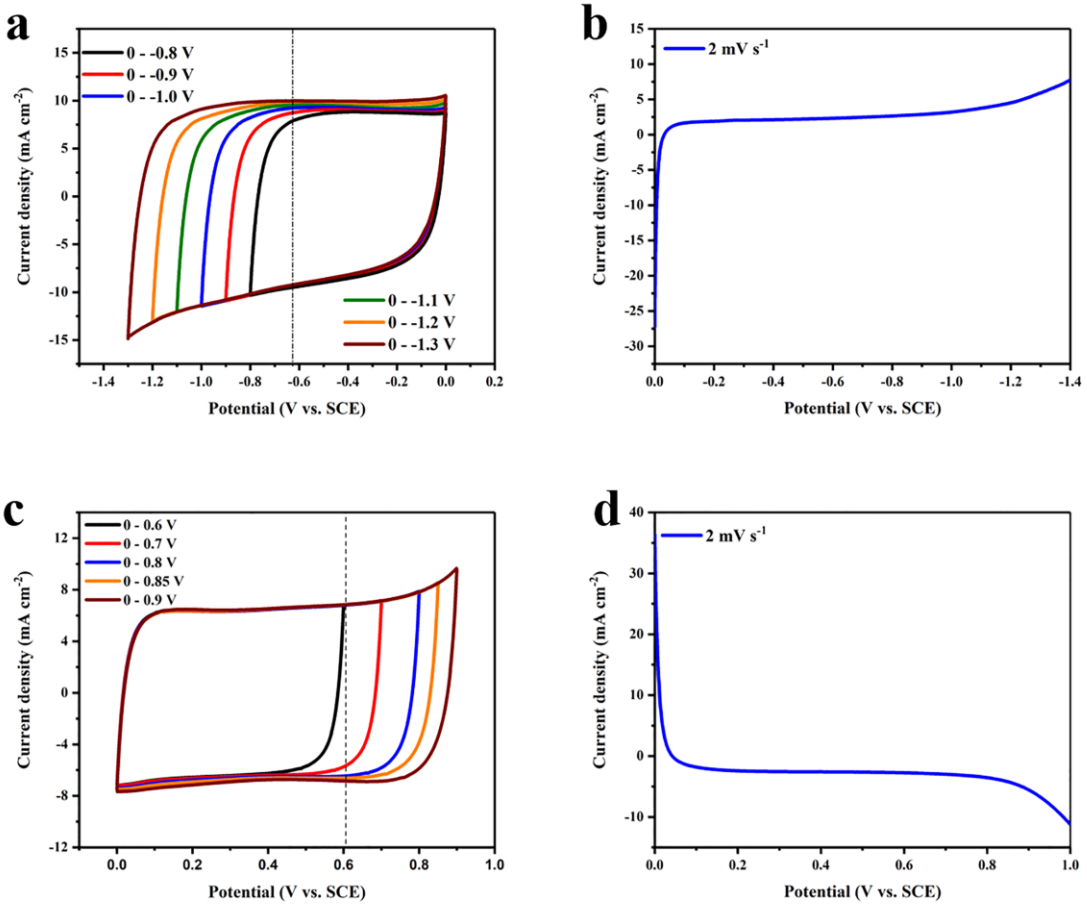

Fig. S16. (a) CV curves of the CC–400 °C–6h electrode in increasing potentials up to -1.3 V. (b) Linear sweep voltammetry (LSV) analysis at 2 mV s^{-1} to study the hydrogen evolution (c) CV curves of the CC–400 °C–6h electrode in increasing potentials up to 0.9 V. (d) LSV analysis at 2 mV s^{-1} to study the oxygen evolution.

The potentials for hydrogen and oxygen evolution are pH-dependent and can be determined from the equations shown below [1]:

$$E_{red} = -0.059\, pH - 0.244\ vs.SCE \quad (1)$$

$$E_{oxid} = 1.23 - 0.059\, pH - 0.244\ vs.SCE \quad (2)$$

The CV curves tested at a scan rate of 5 mV s^{-1} with gradual shift to more negative (Fig. S16 a) and positive potentials (Fig. S16 c) shows that the activated CC is stable beyond the theoretical onset potentials for hydrogen and oxygen evolutions (indicated by a dotted line). The extended potential window is a result of the large hydrogen and oxygen overpotentials of the activated CC in 1 M Na_2SO_4 electrolyte, as confirmed from the LSV curves (Fig. S16 b and d).

The 1 M Na_2SO_4 electrolyte has a neutral pH value close to 7, hence a little amount of hydroxyl (OH^-) anions generated from the water reduction is able to cause an increase of the pH inside the pores of the CC–400 ºC–6h to much higher values and this results in a higher overpotential for di-hydrogen evolution [2, 3]. On the other hand, oxygen evolution reactions (OER) are kinetically sluggish processes which involves multi-step redox reactions between the electrolyte and the oxygen functional groups on the carbon material surface. The sluggish nature of these reactions in the CC–400 ºC–6h electrode results in a large overpotential which suppresses the oxygen evolution beyond the theoretical onset potential (0.606 V vs. SCE). The LSV curves show that the hydrogen and oxygen evolution start beyond -1.2 and 0.85 V vs. SCE, respectively, hence, it is safe to cycle the symmetric electrochemical capacitor device in the wide 2.0 V potential window.

Table S1 Comparison of the XPS elemental composition of the CC-400 ºC-6h electrodes as well as the control samples.

Sample ID	Carbon (at %)	Oxygen (at %)
Pristine CC	95.14	4.86
CC-360 ºC-6h	95.29	4.71
CC-400 ºC-2h	93.97	6.03
CC-400 ºC-6h	87.89	12.11

Table S2 Percentages of oxygen functional groups derived from the deconvoluted O 1s peak.

Carbon Textile Material	C-OH (%)	O-C=O (%)	COOH (%)	C=O
Pristine CC	48.03	29.51	22.46	–
CC-300 ºC-6h	49.68	28.15	22.16	–
CC-400 ºC-2h	25.3	30.87	21.81	21.86
CC-400 ºC-6h	29.04	26.79	17.91	26.27

Table S3 Comparison of the electrochemical performance of the CC-400 ºC-6h electrodes and other carbon textile-based electrodes.

Carbon Textile Material	Electrolyte	Voltage Range (V)	Capacitance (mF cm^{-2})	Capacitance Retention	Cycling Performance
Chemically activated carbon clothes [4]	1 M H_2SO_4	0 – 1.0 V	88 (10 mV s^{-1})	73 % retention at 1000 mV s^{-1}	97 % after 20000 cycles
Electrochemically activated carbon clothes [5]	1 M LiCl	-1.0 – 0 V	756 (6 mA cm^{-2})	65.2 % retention at 20 mA cm^{-2}	Stable cycling up to 30000 cycles
Paper + CNT + MnO_2 [6]	6 M KOH	0 – 1.0 V	123 (1 mA cm^{-2})	–	–
Activated carbon clothes [7]	1 M H_2SO_4	0 – 1.0 V	482.04 (1 mA cm^{-2})	89.7 % retention at 60 mA cm^{-2}	129 % after 30000 cycles
Activated carbon clothes [8]	1 M H_2SO_4	0 – 1.0 V	505 (6 mA cm^{-2})	88 % retention at 48 mA cm^{-2}	97 % after 30000 cycles
Functionalized carbon fabric [9]	0.5 M Na_2SO_4	0 – 0.8 V -0.8 – 0 V	143.4 (1 mA cm^{-2}) 155.8 (1 mA cm^{-2})	91.63 and 88.5 % retention at 20 mA cm^{-2}	–
Hydrothermally activated graphene fiber fabric [10]	1 M H_2SO_4	–	1060 (1 mA cm^{-2})	68 % retention at 100 mA cm^{-2}	Stable up to 50000 cycles
Carbonized cotton mat [11]	1 M Na_2SO_4	0 – 0.8 V	0.7 (0.0112 mA cm^{-2})	92 % retention at 0.112 mA cm^{-2}	–
Graphene cellulose paper [12]	1 M H_2SO_4	0 – 0.8 V	81 (1 mV s^{-1})	–	Stable up to 50000 cycles
Activated carbon cloth [13]	6 M KOH	0 – 1 V	1136.7 (2 mV s^{-1})		Stable cycling up to 50000 cycles
Activated porous carbon fiber textile [14]	5 M LiCl	-1 – 0 V	1200 (4 mA cm^{-2})	59 % at 80 mA cm^{-2}	Stable cycling up to 25000 cycles
CC-400 ºC-6h [This work]	1 M Na_2SO_4	0 – 2 V	1700 (1 mA cm^{-2})	66 % at 65 mA cm^{-2}	Stable cycling up to 20000 cycles

Table S4 Carbon yield after activation.

Sample ID	Before	After
Pristine CC	~14.5 mg cm^{-2}	-
CC-360 ºC-6h	~14.5 mg cm^{-2}	~14.4 mg cm^{-2}
CC-400 ºC-2h	~14.5 mg cm^{-2}	~13.85 mg cm^{-2}
CC-400 ºC-6h	~14.5 mg cm^{-2}	~13 mg cm^{-2}
CC-500 ºC-6h	~14.5 mg cm^{-2}	~0.16 mg cm^{-2}

References

[1] M. Yu, Y. Lu, H. Zheng, X. Lu, Chem.–Eur. J., 24 (2018) 3639-3649.

[2] Y. L. Shao, M. F. El-Kady, J. Y. Sun, Y. G. Li, Q. H. Zhang, M. F. Zhu, H. Z. Wang, B. Dunn, R. B. Kaner, Chem. Rev., 118 (2018) 9233-9280.

[3] K. Fic, G. Lota, M. Meller, E. Frackowiak, Energy Environ. Sci., 5 (2012) 5842-5850.

[4] G. Wang, H. Wang, X. Lu, Y. Ling, M. Yu, T. Zhai, Y. Tong, Y. Li, Adv. Mater., 26 (2014) 2676-2682.

[5] W. Wang, W. Liu, Y. Zeng, Y. Han, M. Yu, X. Lu, Y. Tong, Adv. Mater., 27 (2015) 3572-3578.

[6] L. Dong, C. Xu, Y. Li, Z. Pan, G. Liang, E. Zhou, F. Kang, Q.H. Yang, Adv. Mater., 28 (2016) 9313-9319.

[7] S. Jiang, T. Shi, X. Zhan, H. Long, S. Xi, H. Hu, Z. Tang, J. Power Sources, 272 (2014) 16-23.

[8] D. Ye, Y. Yu, J. Tang, L. Liu, Y. Wu, Nanoscale, 8 (2016) 10406-10414.

[9] H. Jin, Z. Peng, W. Tang, H. Chan, RSC Adv., 4 (2014) 33022-33028.

[10] Z. Li, T. Huang, W. Gao, Z. Xu, D. Chang, C. Zhang, C. Gao, ACS Nano, 11 (2017) 11056-11065.

[11] J. Xue, Y. Zhao, H. Cheng, C. Hu, Y. Hu, Y. Meng, H. Shao, Z. Zhang, L. Qu, Phys. Chem. Chem. Phys., 15 (2013) 8042-8045.

[12] Z. Weng, Y. Su, D.W. Wang, F. Li, J. Du, H.M. Cheng, Adv. Energy Mater., 1 (2011) 917-922.

[13] Y.-J. Gu, W. Wen, J.-M. Wu, J. Mater. Chem. A, 6 (2018) 21078-21086.

[14] Y. Han, Y. Lu, S. Shen, Y. Zhong, S. Liu, X. Xia, Y. Tong, X. Lu, Adv. Funct. Mater. 29 (2018) 1806329.